Editors' Suggestion | Featured in Physics

Self-Kerr Effect across the Yellow Rydberg Series of Excitons in Cu_2O

Corentin Morin,[1] Jérôme Tignon,[1] Juliette Mangeney,[1] Sukhdeep Dhillon,[1] Gerard Czajkowski,[2] Karol Karpiński,[2] Sylwia Zielińska-Raczyńska,[2] David Ziemkiewicz,[2] and Thomas Boulier[1,*]

[1]*Laboratoire de Physique de l'Ecole Normale Supérieure, ENS, Université PSL, CNRS, Sorbonne Université, Université de Paris, 75005 Paris, France*

[2]*Bydgoszcz University of Science and Technology 7 Kaliskiego Ave., 85-796 Bydgoszcz, Poland*

(Received 20 February 2022; revised 4 June 2022; accepted 18 July 2022; published 19 September 2022)

We investigate the nonlinear refraction induced by Rydberg excitons in Cu_2O. Using a high-precision interferometry imaging technique that spatially resolves the nonlinear phase shift, we observe significant shifts at extremely low laser intensity near each exciton resonance. From this, we derive the nonlinear index n_2, present the n_2 spectrum for principal quantum numbers $n \geq 5$, and report large n_2 values of order 10^{-3} mm^2/mW. Moreover, we observe a rapid saturation of the Kerr nonlinearity and find that the saturation intensity I_{sat} decreases as n^{-7}. We explain this with the Rydberg blockade mechanism, whereby giant Rydberg interactions limit the exciton density, resulting in a maximum phase shift of 0.5 rad in our setup.

DOI: 10.1103/PhysRevLett.129.137401

Nonlinear optics has been of paramount scientific importance, unlocking an impressive number of technologies now used in areas ranging from telecommunication and data storage to quantum research. While early studies focused on inorganic crystals as a nonlinear medium, nowadays record nonlinearities are obtained from the coherent manipulation of atomic resonances [1]. In particular, dense ultracold atomic gases excited to a high principal quantum number n (a Rydberg state) can induce strong nonlinearities at the level of individual photons [2,3]. Following in the footsteps of their atomic cousins, Rydberg excitons are attracting considerable attention as they represent an enticing path towards more scalable solid-state Rydberg systems [4], with potential for quantum simulation [5] and photon logic [6,7].

In copper oxide (Cu_2O), the semiconductor where excitons were first discovered, principal quantum numbers up to $n = 30$ were observed [8–10]. These correspond to gigantic electron-hole wave functions that can span several microns in diameter and were confirmed to have the same n scaling as atoms [11]; however, the physical origin of these similarities is quite different due to the complex valence band structure and the different selection rules for excitons. On the one hand, the n^{-3} scaling of linewidths rapidly leads to sharp resonances, near which the nonlinear optical response terms are enhanced. On the other hand, the n^{11} scaling for van der Waals interactions generates a distinct nonlinear optical response due to the phenomenon of Rydberg blockade [8], whereby a single Rydberg exciton prevents the formation of any other within a blockade volume $V_B \propto n^7$ due to the energy cost of dipolar interactions [2]. Rydberg blockade is one of the mechanisms that induces a saturation of the exciton density and therefore a nonlinear optical response, as is well known for the absorption [8,12]). Since signatures of coherence were observed [13], several theoretical studies focused on the optical nonlinearities of Rydberg excitons [14–16] in view of their potential for nonlinear quantum optics [6,7,17,18]. Experimental studies on Rydberg exciton nonlinearities are dominated by second harmonic generation ($\chi^{(2)}$ term) as a potent spectroscopic tool [19–22] and by investigating the blockade-induced nonlinear absorption [8,23,24]. However, so far, no experimental study has looked at the giant Kerr-type optical nonlinearities, whereby the light intensity I modifies the optical index as $n = n_0 + n_2 I$ due to the nonlinear term $n_2 \propto \chi^{(3)}$, expected from the sharp Rydberg resonances [14]. This is in spite of their important role for nonlinear quantum optics, as Kerr nonlinearities are equivalent to photon-photon interactions and have been instrumental both for applications (e.g., Kerr mode-locking [25]) and fundamental investigations [26] (e.g., superfluids of light [27–29], nonlinear photonics [3,30,31]). Indeed, a Kerr nonlinearity operating at the scale of a few photons is key to all-optical quantum information processing, a paramount goal in the current context. Thus, a condensed matter medium supporting giant nonlinear indices is of strong interest, and Rydberg excitons were proposed as a more scalable alternative to ultracold atomic gases [6,18]. Therefore, to map the potential of Rydberg excitons for nonlinear optics, their ability to generate a large Kerr coefficient must be explored.

To this end, we reveal the giant nonlinear optical index caused by the sharp Rydberg resonances and observe a Kerr coefficient up to 10^{14} larger than in typical nonlinear crystals. Moreover, we also observe a rapid saturation of

 © 2022 American Physical Society

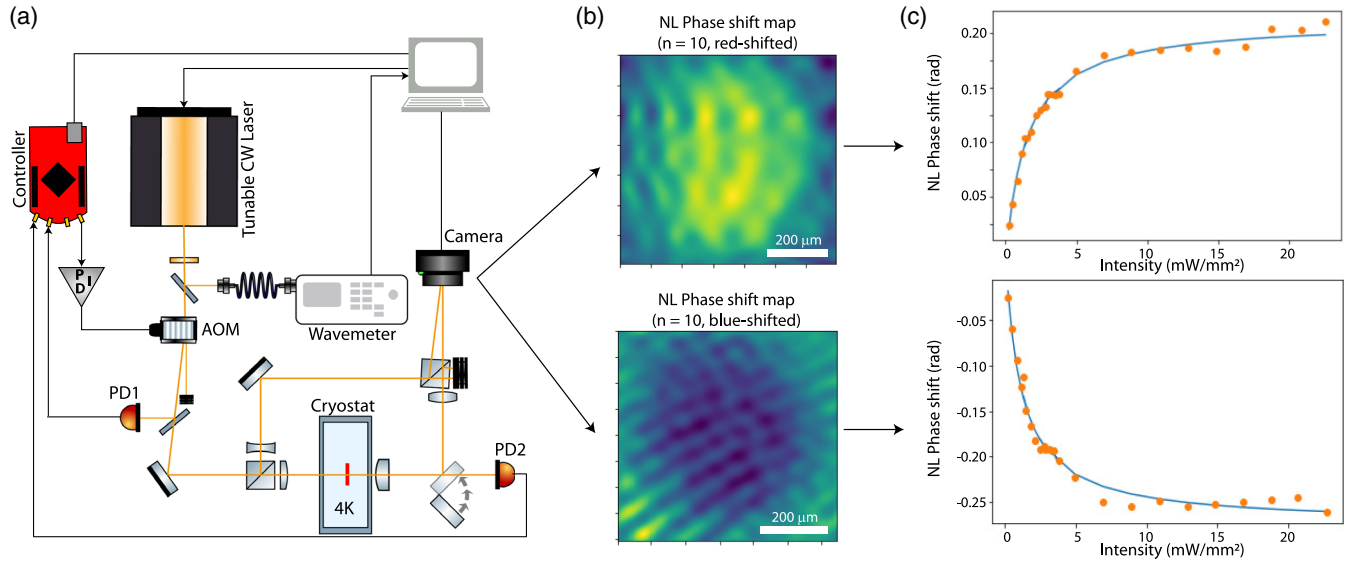

FIG. 1. (a) Simplified view of the experimental apparatus. Acousto-optic modulator (AOM), photodiode (PD). (b) Examples of nonlinear phase shifts reconstructed from interferograms (see Supplemental Material [36]): red-detuned (up) and blue-detuned (down) from the $n = 10$ resonance. The pattern matches the input intensity profile (shown in [36]). (c) Intensity dependence of the phase shift extracted from the intensity and phase pictures. We fit the data with the saturable function $f(I) = [\alpha I/(1 + I/I_{\mathrm{sat}})]$.

the optical nonlinearity at low power, which matches the expectations from Rydberg blockade. While other effects [32–35] may add a minor contribution (see Supplemental Material [36]), including the Rydberg blockade in our model yields an excellent agreement with the experiment. The experimental method is an improved, high-precision variation of interferometric phase front imaging [44] able to accurately map small Kerr phase shifts. While it does not quite reach the quantum regime of a few photons, the present investigation of nonlinear refraction in Cu_2O provides a complimentary insight to the previous nonlinear absorption studies.

Figure 1(a) is a simplified representation of the experiment. The sample is a 50 μm thick natural Cu_2O crystal, highly polished on both sides and oriented so that light propagates along the [001] axis. It is held strain-free in a 4 K cryostat in the transmission mode. A spectrally narrow CW yellow laser is focused on the sample with a waist diameter of about 400 μm. Both the laser frequency and intensity are stabilized with PID feedback loops. The latter is important for our highly nonlinear system and allows us to modulate the laser to avoid heating. The transmission is measured during a single 10 ms pulse by a pair of amplified photodiodes. A motorized flip mirror switches between the transmission measurement and the imaging system that spatially resolves the transmitted intensity and phase. The main computer orchestrates a fully automated measurement protocol, including quality assessment routines.

We image the phase front of the transmitted beam using a modified Mach-Zehnder interferometer. One arm is focused on the sample and imaged on a camera, while the other is expanded and used as a quasiflat reference. The sample image and the reference arrive on the camera at an angle so that high-contrast fringes containing the phase information are present in the raw picture (shown in the Supplemental Material [36]). The phase picture is then retrieved numerically with a Fourier transform algorithm (described in [36]). Both the interference pattern and the intensity profile are captured using shutters. Moreover, for each laser energy we typically take two sets of pictures: one at the desired laser power P and one at vanishing laser power (at least 50× lower than P). The low-power data contain a negligible amount of nonlinear phase shift compared with the high-power data. We therefore subtract the low-power phase profile from the high-power phase profile to ensure that only intensity-dependent effects remain. The final nonlinear phase shift map is exemplified in Fig. 1(b), while the raw interferograms and the image processing steps are shown in detail in the Supplemental Material [36]. Such subtraction of the linear phase profile has the advantage of neatly removing systematic imperfections (e.g., the residual parabolic phase front of the reference beam and small optical aberrations) and was found crucial to reach a sufficient resolution for our Cu_2O system. Another important noise source is the air fluctuations, which we reduced by carefully shielding our small interferometer and by integrating each image for longer than the dominant fluctuation timescale ($\lesssim$100 ms). The typical phase resolution of our setup is of order ± 0.01 rad.

The Gaussian profile of the input beam (shown in the Supplemental Material [36]) contains all intensities between zero and its maximum $I_{\mathrm{max}} = P/(2\pi\sigma^2)$, where $\sigma = 200$ μm is the Gaussian radius. Therefore, the

self-Kerr effect induces a nonuniform nonlinear phase shift pattern [see Fig. 1(b)] roughly resembling the input intensity profile. We extract the phase shift dependence on the input intensity $\Delta\phi(I)$ from the intensity and phase images by calculating the average phase shift for sets of pixels containing the same intensity. Figure 1(c) presents examples of $\Delta\phi(I)$ for two different energies, red- and blue-detuned from the $n = 10$ exciton resonance. As the sign of the real part of susceptibility is either negative or positive depending on the photon-exciton detuning, the Kerr coefficient changes sign between these examples. We report here the maximum observed phase shift, the nonlinear optical index n_2 deduced from the initial slope $(\partial\Delta\phi/\partial I)|_{I\to 0}$ and the saturation intensity I_{sat} typically observed near exciton resonances.

This approach has significant advantages over the traditional z-scan technique [45]. It does not need a perfect Gaussian beam because we spatially resolve both the intensity and phase signals. It is therefore robust to optical aberrations. Additionally, our approach does not require moving parts: it is faster, more stable and, importantly, compatible with complex setups that cannot be moved, such as cryostats (as is the case here). It is typically more precise and it is cost effective: the most expansive part is the camera, which does not need to be especially fast or sensitive. Moreover, we directly access the phase shift $\Delta\phi(I)$: the measured quantity is physically relevant and the fitting is simple, revealing both n_2 and I_{sat}. Finally, unlike with the z-scan technique, focusing the laser is not necessary and this technique is compatible with a wider class of systems where focusing is not possible. While a few previous studies used interferometers [44,46–48], they typically did not exploit images [44] or they relied on a pump-probe approach [46–48] (cross-Kerr effect) that would complicate the high-precision resonant nonlinear spectroscopy presented here. Moreover, we note that in parallel to our work an equivalent single-beam method has been developed, benchmarked, and used on a single, non-Rydberg resonance in hot atomic vapors [49]. Importantly for our system, we significantly improved the phase resolution (e.g., $\times 2$ relative to Ref. [46] and $\times 10$ relative to Ref. [49]).

Nonlinear effects in excitonic spectra can be modeled in the framework of the so-called real density matrix approach (RDMA) [14]. The RDMA provides analytical expressions for the optical response of any semiconductor crystal using a small number of well-known parameters (e.g., effective masses, gap energy, dielectric constant). It can include Rydberg excitons of arbitrarily high principal quantum numbers, includes the case of indirect interband transitions, takes into account the effects of an anisotropic dispersion and the coherence of the electron and the hole with the radiation field. The total refraction index for an average intensity I inside a crystal of the length L is given by $n^2 = \epsilon_b + \chi^{(1)} + \chi^{(3)}(I)$, where $\chi^{(1)}$ and $\chi^{(3)}(I)$ are the linear and nonlinear parts of the susceptibility, allowing one to calculate the nonlinear phase shift $\Delta\phi = (\omega L/c)[n(I) - n(0)]$. The analytical expressions for the linear and nonlinear susceptibilities are derived in the Supplemental Material [36], where several strategies are discussed to take into account the Rydberg blockade effect. While several method were put forward to take exciton-exciton interactions [6,14,16,50], one crude approach is to treat exciton-exciton interactions as a broadening mechanism, from which the known Rydberg scaling laws [11] correctly lead to the prediction of a saturation density decreasing as n^{-7} on resonance. A complementary approach consists in using a saturable function $f(I) = [\alpha I/(1 + I/I_{\mathrm{sat}})]$ to scale either the constant $\chi_0^{(3)}$ or the oscillator strengths $\mathcal{F}_{nn'}$, mimicking the blockade. While both approaches qualitatively match the experiment (see Supplemental Material [36]), they predict different line shapes. As the line shapes predicted by the saturable approach agrees better with the experiment, we favored it in the theoretical plot shown here.

Figure 2(a) presents the absorption spectrum as a function of the energy difference between the probe light and the gap $\Delta E = E_{\mathrm{gap}} - \hbar\omega$ ($E_{\mathrm{gap}} = 2.1721$ eV),

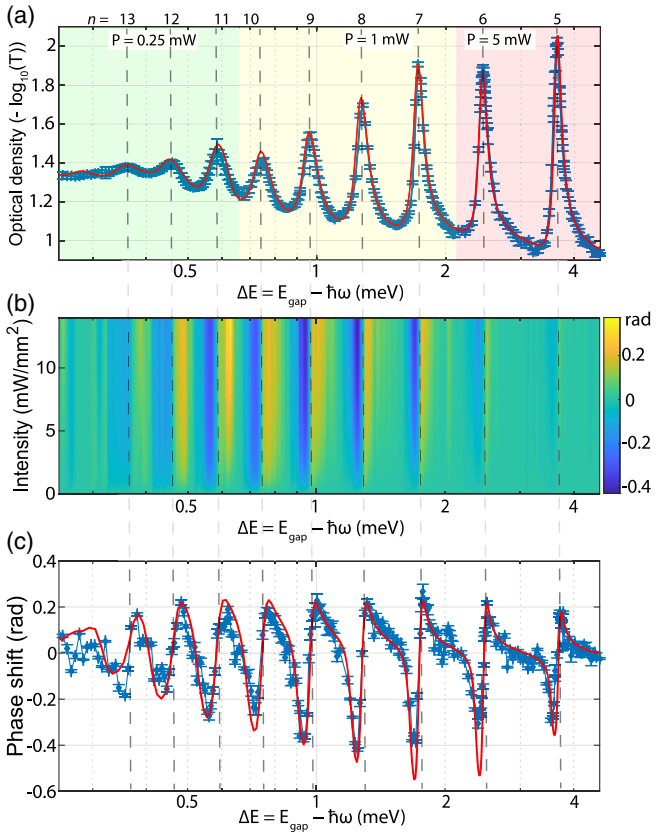

FIG. 2. (a) Optical density spectrum of the yellow Rydberg series, plotted versus the energy difference between the probe light and the gap $\Delta E = E_{\mathrm{gap}} - \hbar\omega$. Blue dots: experimental data (incl. error bars), red line: theory. Different powers were used for different states. (b) Color map of the nonlinear phase shift, plotted against ΔE and the intensity. (c) Maximum (saturated signal) nonlinear phase shift. Blue dots: experimental data (incl. error bars), red line: theory.

obtained by measuring the sample transmission at various energies $\hbar\omega$. Principal quantum numbers up to $n = 13$ are clearly observed. Fitting our model indicates a constant 12 μeV broadening of all excitonic lines. Our estimates point to charged impurities as the main reason for this broadening [33]. Because of the extreme n dependence of the nonlinear absorption [8], different laser powers were used for different states to avoid bleaching the high n while keeping a sufficient signal across the large absorption of the low-n peaks, as the color code in Fig. 2(a) indicates. As nonlinear dissipation has already been thoroughly studied in Cu_2O [6,16], here we focus instead on the nonlinear dispersion. Figure 2(b) is an example of observed self-Kerr phase shifts in the energy-intensity plane, enlarged on low laser intensities (0–14 mW/mm^2). As is visible by the increase of signal with n, higher states require less intensity to induce a phase shift. Additionally, the maximum phase shift $\Delta\phi_{\max}$ spectrum is presented in Fig. 2(c). It is maximum in the sense that we ensure saturation is reached: $\Delta\phi_{\max} = \Delta\phi(I \gg I_{\rm sat}) - \Delta\phi(0)$ and the system cannot produce larger shifts regardless of the power used. We observe the typical positive-negative phase shift around each Rydberg state, with a sharp zero crossing exactly on resonance. The peak-to-peak amplitude first grows slowly with n due to the increased nonlinear optical index n_2. It then decreases to completely vanish at $n = 14$. This is in good agreement with the observed broadening of the $n = 11$–13 states and the absence of $n = 14$ in the absorption. While $\Delta\phi_{\max}$ has modest values of order ± 0.25 rad, it is obtained at extremely low input intensities of order 1 mW/mm^2 around $n = 10$. This is indicative of an extremely large nonlinearity near resonance, albeit one that saturates quickly.

As saturation is present for all states beyond some intensity $I_{\rm sat}$, we fit $\Delta\phi(I)$ with a saturable function $f(I) = [\alpha I/(1 + I/I_{\rm sat})]$ for each laser energy $\hbar\omega$. The nonlinear index n_2 is calculated from the fit parameter α while the saturation intensity $I_{\rm sat}$ is obtained directly.

Nonlinear index.—In a transparent medium far from saturation, the nonlinear phase shift is $\Delta\phi(I) = kLIn_2$, where $k = (2\pi/\lambda)$ is the light wave vector. Therefore, $n_2 = (1/kL)(\partial\Delta\phi/\partial I)|_{I \ll I_{\rm sat}} = (\alpha/kL)$. However, Cu_2O is not transparent and one has to take into account the reduced intensity inside the crystal. Rather than taking into account the full nonlinear intensity variation $I(z)$ along the propagation axis z, we make the approximation of a linear absorption $I(z) = I_0 e^{-z/z_0}$, where z_0 is the linear absorption length. This is justified as $\alpha = (\partial\Delta\phi/\partial I)|_{I_0 \to 0}$ is the derivative of $\Delta\phi(I)$ taken in the low intensity limit where nonlinear absorption is negligible. In that case we find $n_2 = (\alpha/kz_0)$, where $z_0 = -(L/\ln T) < L$ is inversely proportional to the optical density measured at low power. The resulting $n_2(\hbar\omega)$ spectrum is shown in Fig. 3(a). Interestingly, the peak-to-peak n_2 amplitude rapidly increases with n and reaches a maximum at $n = 10$ of order $n_2 = 10^{-3}$ mm^2/mW. This is about 2–4 orders of magnitude larger than in typical atomic systems [49,51,52] and 14 orders of magnitude beyond typical nonlinear crystals. For $n \geq 11$ the measured n_2 falls off, likely due to the broadening from charged impurities. Note that here the $n = 14$ signal is present, unlike in the optical density data: as extracting n_2 only requires the low-intensity part of the pictures (0–0.5 mW/mm^2 for $n = 14$) we infer that, on top of being broadened by thermal phonons, $n = 14$ is at least partly blockaded in Fig. 2(a) and saturates too fast to show a significant signal in Figs. 2(b)–2(c).

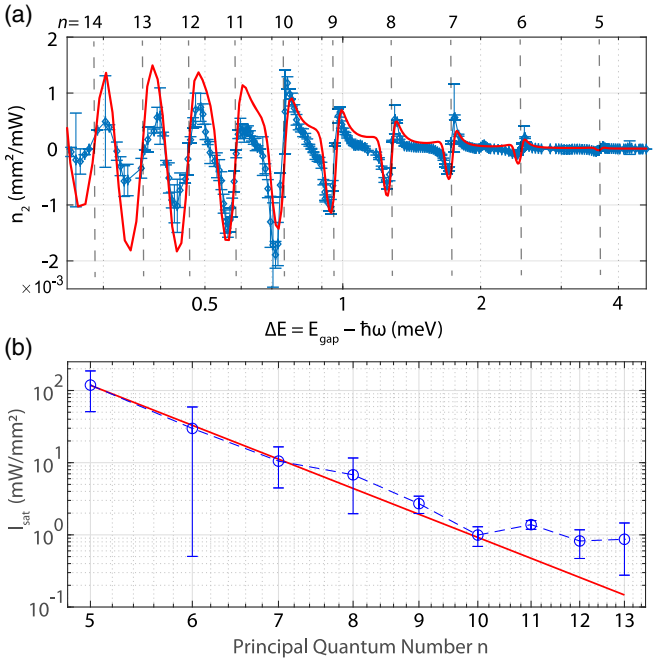

FIG. 3. (a) Nonlinear index n_2 extracted form the low-power derivative of $\Delta\phi(I)$. Blue dots: experimental data (including error bars), red line: theory. Note that here the state $n = 14$ is visible. (b) The power law fit (red line) of $I_{\rm sat}(n)$ (blue dots) indicates an exponent of -6.9 ± 0.2.

Saturation.—The saturation intensity $I_{\rm sat}(\omega)$ varies rapidly with the energy, going from $I_{\rm sat} \to \infty$ far from resonance to a local minimum $I_{\rm sat}^{\rm min}$ around each resonance, as is typical of saturable systems. We focus here on the vicinity of $I_{\rm sat}^{\rm min}$ as its variation with n brings interesting insights. We define $I_{\rm sat}(n) = \langle I_{\rm sat}(\omega)\rangle_n$, where $\langle\ldots\rangle_n$ is the average over ω within a FWHM of the nP absorption peak. As visible in Fig. 3(b), $I_{\rm sat}(n)$ is of order 100 mW/mm^{-2} for $n = 5$ but decreases rapidly, reaching $I_{\rm sat} \lesssim 1$ mW/mm^{-2} for $n \geq 10$. This is similar to the saturation intensity observed in our absorption. To find the origin of this behavior, we fit a power law $A(n - \delta_\ell)^b$, where $\delta_{\ell=1} = 0.23$ is the quantum defect for P states in Cu_2O [8], a correction originating from the band anharmonicity. The exponent is found to be $b = -6.9 \pm 0.2$. This suggests the rapid saturation is a Rydberg blockade effect. Indeed, the total Kerr shift depends on the real part of susceptibility, which is

proportional to the exciton density. However, due to the Rydberg blockade, the exciton density saturates and its maximum is the inverse blockade volume, $\rho_{\max} = 1/V_B \propto n^{-7}$ [8]. Therefore, Rydberg blockade implies that the Kerr shift saturates at some intensity $I_{\text{sat}} \propto \rho_{\max} \propto n^{-7}$, as observed.

In conclusion, we measure the saturable nonlinear refraction induced by Rydberg excitons in Cu_2O. Our approach is radically different from the traditional z-scan technique: by directly imaging the Kerr-induced phase shift $\Delta\phi(I)$, we simultaneously access the nonlinear index n_2 and the saturation intensity I_{sat}. We reach the high precision of ± 0.01 rad, allowing to resolve our relatively small signal. Interestingly, $\Delta\phi$ always remains small in spite of the gigantic n_2 values reached at high principal quantum number because of a rapid saturation. We find this saturation is due to the Rydberg blockade [8] inducing a saturation intensity $I_{\text{sat}} \propto n^{-7}$, which hinders large phase shifts. Incorporating this observed saturation into the model developed in Ref. [14] yields excellent agreement between the theoretical predictions and the experimental results. To the best of our knowledge, electromagnetically induced transparency (EIT) in cold atoms [1–3,53] is the only scheme that has displayed a Kerr coefficient larger than the value of 10^{-3} mm^2/mW reported here.

Our results therefore underline that Rydberg excitons are a strong candidate for solid-state nonlinear quantum optics. While Rydberg blockade and absorption are a limitation in our single-pump study, the situation would be completely different with a two-colors strategy (simultaneously coupling three levels) in the fashion of Rydberg EIT [2,3]: the absorption would be suppressed while the blockade would massively enhance the Kerr coefficient, rather than hinder it. Therefore, EIT has the potential to reach the quantum regime of Kerr nonlinearity, unlike single-pump approaches. Recent theoretical studies pave the way toward such goals [6,7], using both intraseries [18] and interseries [54,55] Rydberg exciton transitions, including the nontrivial role of phonons [15]. With promising new results for intraseries coupling in the microwave domain [24] and recent advances in THz sources [56,57] enabling us to explore transitions in the 1–10 meV range, experimentally probing two-photon strategies is likely to soon yield important results for solid-state Rydberg physics.

We thank Quentin Glorieux and Murad Abuzarli for useful discussions. This work has been supported by the ANR Grant No. ANR-21-CE47-0008 (PIONEEReX).

*thomas.boulier@phys.ens.fr

[1] M. Fleischhauer, A. Imamoglu, and J. P. Marangos, Rev. Mod. Phys. **77**, 633 (2005).
[2] A. V. Gorshkov, J. Otterbach, M. Fleischhauer, T. Pohl, and M. D. Lukin, Phys. Rev. Lett. **107**, 133602 (2011).
[3] T. Peyronel, O. Firstenberg, Q.-Y. Liang, S. Hofferberth, A. V. Gorshkov, T. Pohl, M. D. Lukin, and V. Vuletić, Nature (London) **488**, 57 (2012).
[4] M. Aßmann and M. Bayer, Adv. Quantum Technol. **3**, 1900134 (2020).
[5] J. Taylor, S. Goswami, V. Walther, M. Spanner, C. Simon, and K. Heshami, Quantum Sci. Technol. **7**, 035016 (2022).
[6] V. Walther, R. Johne, and T. Pohl, Nat. Commun. **9**, 1309 (2018).
[7] V. Walther, L. Zhang, S. F. Yelin, and T. Pohl, Phys. Rev. B **105**, 075307 (2022).
[8] T. Kazimierczuk, D. Fröhlich, S. Scheel, H. Stolz, and M. Bayer, Nature (London) **514**, 343 (2014).
[9] J. Heckötter, D. Janas, R. Schwartz, M. Aßmann, and M. Bayer, Phys. Rev. B **101**, 235207 (2020).
[10] M. A. M. Versteegh, S. Steinhauer, J. Bajo, T. Lettner, A. Soro, A. Romanova, S. Gyger, L. Schweickert, A. Mysyrowicz, and V. Zwiller, Phys. Rev. B **104**, 245206 (2021).
[11] J. Heckötter, M. Freitag, D. Fröhlich, M. Aßmann, M. Bayer, M. A. Semina, and M. M. Glazov, Phys. Rev. B **96**, 125142 (2017).
[12] J. Heckötter, M. Freitag, D. Fröhlich, M. Aßmann, M. Bayer, P. Grünwald, F. Schöne, D. Semkat, H. Stolz, and S. Scheel, Phys. Rev. Lett. **121**, 097401 (2018).
[13] P. Grünwald, M. Aßmann, J. Heckötter, D. Fröhlich, M. Bayer, H. Stolz, and S. Scheel, Phys. Rev. Lett. **117**, 133003 (2016).
[14] S. Zielińska-Raczyńska, G. Czajkowski, K. Karpiński, and D. Ziemkiewicz, Phys. Rev. B **99**, 245206 (2019).
[15] V. Walther, P. Grünwald, and T. Pohl, Phys. Rev. Lett. **125**, 173601 (2020).
[16] V. Walther and T. Pohl, Phys. Rev. Lett. **125**, 097401 (2020).
[17] M. Khazali, K. Heshami, and C. Simon, J. Phys. B **50**, 215301 (2017).
[18] D. Ziemkiewicz, Entropy **22**, 177 (2020).
[19] A. Farenbruch, D. Fröhlich, D. R. Yakovlev, and M. Bayer, Phys. Rev. Lett. **125**, 207402 (2020).
[20] J. P. Rogers, L. A. Gallagher, D. Pizzey, J. D. Pritchett, C. S. Adams, M. Jones, C. Hodges, W. Langbein, and S. A. Lynch, Phys. Rev. B **105**, 115206 (2022).
[21] J. Mund, D. Fröhlich, D. R. Yakovlev, and M. Bayer, Phys. Rev. B **98**, 085203 (2018).
[22] A. Farenbruch, D. Fröhlich, H. Stolz, D. R. Yakovlev, and M. Bayer, Phys. Rev. B **104**, 075203 (2021).
[23] J. Heckötter, V. Walther, S. Scheel, M. Bayer, T. Pohl, and M. Aßmann, Nat. Commun. **12**, 3556 (2021).
[24] L. A. P. Gallagher, J. P. Rogers, J. D. Pritchett, R. A. Mistry, D. Pizzey, C. S. Adams, M. P. A. Jones, P. Grünwald, V. Walther, C. Hodges, W. Langbein, and S. A. Lynch, Phys. Rev. Research **4**, 013031 (2022).
[25] T. Brabec, C. Spielmann, P. Curley, and F. Krausz, Opt. Lett. **17**, 1292 (1992).
[26] W. Schäfer and M. Wegener, *Semiconductor Optics and Transport Phenomena* (Springer Science & Business Media, Springer Berlin, 2013).
[27] I. Carusotto and C. Ciuti, Rev. Mod. Phys. **85**, 299 (2013).
[28] Q. Fontaine, T. Bienaimé, S. Pigeon, E. Giacobino, A. Bramati, and Q. Glorieux, Phys. Rev. Lett. **121**, 183604 (2018).

[29] T. Boulier, M. J. Jacquet, A. Maître, G. Lerario, F. Claude, S. Pigeon, Q. Glorieux, A. Amo, J. Bloch, A. Bramati *et al.*, Adv. Quantum Technol. **3**, 2000052 (2020).
[30] D. E. Chang, V. Vuletić, and M. D. Lukin, Nat. Photonics **8**, 685 (2014).
[31] M. Combescot and S.-Y. Shiau, *Excitons and Cooper Pairs: Two Composite Bosons in Many-Body Physics* (Oxford University Press, New York, 2016).
[32] H. Stolz and D. Semkat, J. Phys. Condens. Matter **33**, 425701 (2021).
[33] S. O. Krüger, H. Stolz, and S. Scheel, Phys. Rev. B **101**, 235204 (2020).
[34] H. Stolz, D. Semkat, R. Schwartz, J. Heckötter, M. Aßmann, W.-D. Kraeft, H. Fehske, and M. Bayer, Phys. Rev. B **105**, 075204 (2022).
[35] H. Stolz, R. Schwartz, J. Heckötter, M. Aßmann, D. Semkat, S. O. Krüger, and M. Bayer, Phys. Rev. B **104**, 035206 (2021).
[36] See Supplemental Material at http://link.aps.org/supplemental/10.1103/PhysRevLett.129.137401, which contains Refs. [37–43] for a detailed description of the experimental procedure and the theoretical model.
[37] D. D. Kang, A. Gross, Y. H. Bong, Y. Morita, K. S. Choi, K. Yoshioka, and N. Y. Kim, Phys. Rev. B **103**, 205203 (2021).
[38] J. Thewes, J. Heckötter, T. Kazimierczuk, M. Assmann, D. Fröhlich, M. Bayer, M. A. Semina, and M. M. Glazov, Phys. Rev. Lett. **115**, 027402 (2015).
[39] A. Stahl and I. Balslev, *Electrodynamics of the Semiconductor Band Edge* (Springer-Verlag, Berlin, 1987).
[40] D. Ziemkiewicz and S. Zielińska Raczyńska, Opt. Express **27**, 16983 (2019).
[41] D. Ziemkiewicz, K. Karpiński, G. Czajkowski, and S. Zielińska-Raczyńska, Phys. Rev. B **101**, 205202 (2020).
[42] S. Okumura and T. Ogawa, Phys. Rev. B **65**, 035105 (2001).
[43] K. Orfanakis, S. K. Rajendran, H. Ohadi, S. Zielińska-Raczyńska, G. Czajkowski, K. Karpiński, and D. Ziemkiewicz, Phys. Rev. B **103**, 245426 (2021).
[44] G. Olbright and N. Peyghambarian, Appl. Phys. Lett. **48**, 1184 (1986).
[45] M. Sheik-Bahae, A. A. Said, and E. W. Van Stryland, Opt. Lett. **14**, 955 (1989).
[46] G. Boudebs, M. Chis, and X. N. Phu, J. Opt. Soc. Am. B **18**, 623 (2001).
[47] L. Rodríguez, C. Simos, M. Sylla, A. Marcano O., and X. N. Phu, Opt. Commun. **247**, 453 (2005).
[48] I. Dancus, S. T. Popescu, and A. Petris, Opt. Express **21**, 31303 (2013).
[49] T. Aladjidi, M. Abuzarli, G. Brochier, T. Bienaimé, T. Picot, A. Bramati, and Q. Glorieux, arXiv:2202.05764.
[50] S. Okumura and T. Ogawa, Phys. Rev. B **65**, 035105 (2001).
[51] C. F. McCormick, D. R. Solli, R. Y. Chiao, and J. M. Hickmann, Phys. Rev. A **69**, 023804 (2004).
[52] S. Wang, J. Yuan, L. Wang, L. Xiao, and S. Jia, Opt. Express **28**, 38334 (2020).
[53] L. V. Hau, S. E. Harris, Z. Dutton, and C. H. Behroozi, Nature (London) **397**, 594 (1999).
[54] S. O. Krüger and S. Scheel, Phys. Rev. B **100**, 085201 (2019).
[55] P. Rommel, J. Main, S. O. Krüger, and S. Scheel, Phys. Rev. B **104**, 085204 (2021).
[56] C. A. Curwen, J. L. Reno, and B. S. Williams, Nat. Photonics **13**, 855 (2019).
[57] Y. Wu, Y. Shen, S. Addamane, J. L. Reno, and B. S. Williams, Opt. Express **29**, 34695 (2021).